Comparison of Lidar/Radar Ice cloud parameter retrievals with in-Situ Measurements.

D.P. Donovan and A.C.A.P. Van Lammeren, KNMI, De Bilt, the Netherlands (donovan@knmi.nl)

R. Hogan, Dept. of Meteorology, University of Reading, UK.

P. Francis, UK meteorological Office, Met. Research flights, Farnborough, U.K.

J. Testud, IPSL Centre d'étude des Environnements Terrestre et Planétaires, Vélizy, France

J. Pelon, IPSL–Service d'Aéronomie, Paris, France.

M. Quante, GKSS, Institute for Atmospheric Physics, Geesthach, Germany

J. Goddard, Rutherford Appleton Laboratory, UK

Abstract

The results of a newly developed lidar/radar cloud sounding technique are compared with in-situ measurements made using aircraft mounted 2d probe particle-sizing measurements. Comparisons are presented for two days during the CLARE98 multi-sensor cloud measurement campaign when ice-clouds were sampled. For both days, the remotely derived cloud properties are in good qualitative and quantitative agreement with the in-situ results.

Introduction

During CLARE98, several flights of the UK meteorological office C-130 aircraft were conducted [Francis, 1999]. The C-130 mounted several in-situ particle sizing instruments including 2D-C and 2D-P probes. These instruments are, in principle, capable of measuring the effective size of ice-crystals and to infer the ice-water content of the sampled cloudy volume. Recently, a new procedure for estimating cloud particle effective size and water content profiles using combined lidar and radar data was proposed and has been applied to CARE98 data.

In this paper, comparisons between the C-130 2D probe measurements and the results of both ground and aircraft based lidar/radar cloud soundings are presented for two days during the CLARE98 campaign. For two overflights of the UKMO C-130 on October 21st, results are shown which use the combination of the ground-based GKSS 94GHz radar and the Viasala CT-75K 905 nm lidar celiometer. For October 20th, comparisons between the lidar/radar inversion results using the airborne KESTREL 94 GHz radar together with the LEANDRE 532nm (both mounted on the ARAT aircraft) and in-situ measurements made during a near coincident C-130 flight are presented.

Algorithm

The lidar/radar algorithm that is employed here is the same as that described in Donovan et al. (1999) except that multiple scattering has been accounted for in an approximate fashion using the formalism described in Eloranta (1998). To a large degree, the contribution of multiply scattered light to the observed lidar signal depends on the angular width of the forward scattering lobe of the cloud particle's phase function compared with the field-of-view of the lidar receiver. The width of the forward scattering lobe is, in turn, related to the cross-sectional area of the cloud particles. In general, the larger the particles are the narrower the forward scattering lobe is.

If multiple scattering is ignored, then the retrieved extinction will be lower than the true extinction. Simulations made using both a Monte-Carlo model and the approximate model of Eloranta have shown that for the measurements of ice-clouds made using the CT-75K lidar this effect is generally expected to be below 10-20 % since the field of this instrument is less than 0.6 mrads. For the airborne LEANDRE lidar, with a 3.5 mrad fov, the measured extinction will be only about half the true extinction.

To account for multiple scattering effects, first an inversion is performed assuming no multiple scattering, then the retrieved extinction profile and particle sizes are used to estimated the multiple scattering contribution (to 3rd or 4th order). To do this, the angular width is the forward scattering peak is estimated using the derived *lidar/radar effective radius* (R'_{eff}) [Donovan et al. (1999)] profile together with diffraction theory. Once the multiple scattering contribution has been estimated as a function of range from the lidar the single scattered power can be estimated. When this is done, an inversion is performed on the estimated single-scatter only signal. The multiple scattering contribution is then re-estimated as before and another inversion is then performed. The process is then repeated until the estimated single-scatter power only profile has converged.

A schematic view of the inversion procedure (including multiple scattering effects) is outlined in Fig. 1. The basic method used to determine the inversion far-end boundary value (in R'_{eff}) is the same as that previously described [Donovan and Lammeren, (1999)]. In brief, once $R'_{eff}(z_m)$ is specified and a Klett-type inversion performed, it is possible to calculate what the effective value of C_{lid} must have been (assuming that the radar calibration is reasonable well known). In effect, the inversion procedure performs a number of different Klett-type inversions each with a different boundary value and then chooses the boundary value which gives the smoothest retrieved R'_{eff} profile which corresponds to a feasible value of C_{lid}.

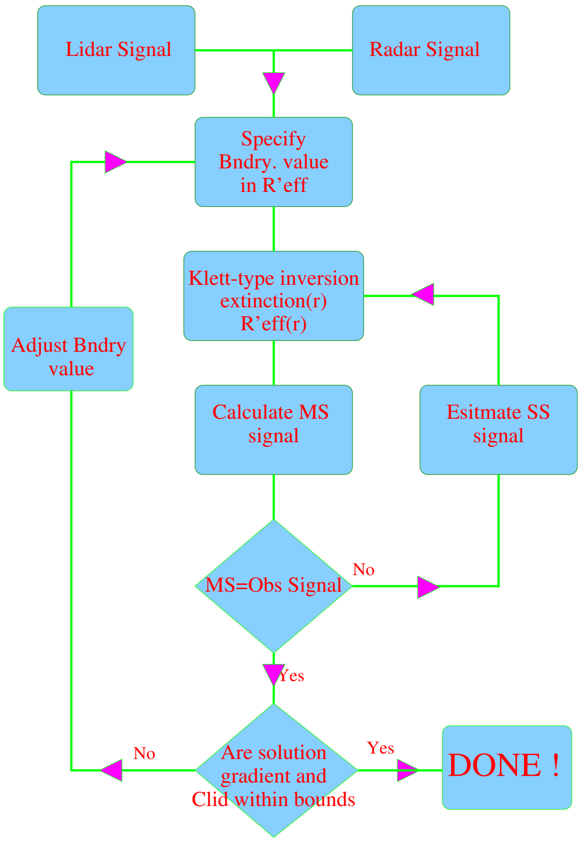

Figure 1: Schematic representation of the lidar/radar inversion procedure including multiple scattering effects.

October 21st

On this day the UKMO C-130 passed over the Chilbolton site four times at an altitude of around 5.8 km. Two of the overpasses occurred around 10:20 Hrs. UTC and two around 10:50 Hrs. UTC. Throughout the campaign a ground-based Viasala CT-75K 905nm lidar was in continuous operation [Goddard (1999)]. During the aircraft flight times, the GKSS 94 GHz radar and the Rablies 35GHz radar were mainly operating in a scanning mode, but they also obtained vertically pointing 'snap-shots' around the direct overpass times. Here the GKSS radar data was chosen for comparison with the lidar due to the higher spatial resolution of the snap-shot data. Details of the GKSS radar are described in Danne and Quante (1999).

The Viasala CT-75K lidar signal along with the effective reflectivity observed by the GKSS radar are shown in Fig. 2. The radar signal here is a snap-shot of around 10 seconds while the lidar signal is an average of about 1.5 minutes. The raw CT-75K measurements have a temporal resolution of 30 seconds and averaging beyond this was found to be necessary. This was due to the relatively low signal-to-noise ratio of the lidar signal and the sporadic detection of the cloud layer between 5.5 and 7km by the lidar celiometer. Figure 2 also shows the ice-water content (IWC) and R'_{eff} profiles derived for the lidar and radar signals together with the values estimated for the IWC and *normal effective radius* ($R_{eff} = 3/4 < mass/\rho_s > / < area >$) from the 2D probe data at around 5.8 km during the overpass.

The lidar/radar derived masses and R_{eff} values were estimated from the reflectivity profiles along with the derived R'_{eff} profile assuming the complex-polycrystal model relationship between particle mass and cross-sectional area of Mitchel et al. (1996), while the 2D probe estimates were made using two different methods. One method uses an empirical relationship between the particle mass and its crossectional area as determined by the probe. The other method uses a relationship between the mass and average mean dimension of the particles. These two methods tend to agree for smaller particles but diverge for larger particle sizes. It can be seen that the values for the ice-water content estimated using the lidar/radar inversion are consistent with the 2D probe estimates. In this figure it can be seen that the effective radii estimates at 5.8 km seem consistent within their respective uncertainties. For both the IWC estimate and the effective size estimate the lidar/radar results tend to agree better with the area-derived 2D probe estimates.

The results for a later overpass are shown in Figure 3. Here, it appears that the aircraft sampled near the top of the cloud. The agreement here is seen not to be as good as for the earlier overpass, particularly with regards to the effective size estimates. However, given the variability of the clouds at this time and the somewhat miss-matched temporal resolutions of the lidar and

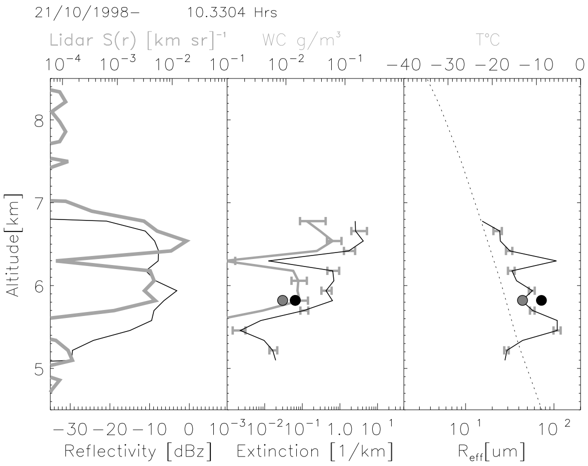

Figure 2: Lidar (Grey) and radar (thin Black) signal profiles for October 21, 1996 at 10.33 Hrs UTC (left). The middle panel shows the retrieved 905 nm extinction profile and estimated IWC profile (Grey) while the right panel shows the retrieved R_{eff} profile and the UKMO temperature profile (upper -axis). The black circles denote the values inferred from the C-130 mounted 2D probes using the mass-vs-area relationship while the Grey dots show the respective estimate made using the mass-vs-maximum average dimension relationship.

radar data used here it is hard to attach too much significance to the disagreement (or even agreement) between the lidar/radar and in-situ results in this and the previous case.

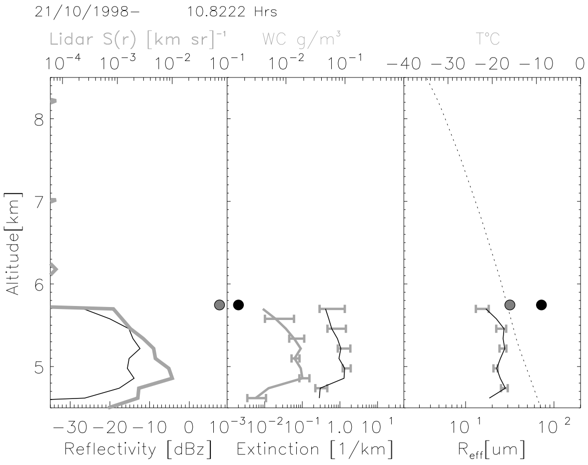

Figure 3: As Fig. (2) except for 10.83 Hrs UTC.

October 20th

On October 20th a near coincident flight path was flown by the French ARAT aircraft and the UKMO C-130. The ARAT carried the LEANDRE 532nm lidar along with the KESTREL 94 GHz Radar. Details of the two instruments can be found in Guyot et al., (1999a) and Guyot et al., (1999b). The observed lidar reflectivites and backscatter signals for this flight are shown in the upper panels of Fig. (4). Here a large cloud is visible in the top right portion of both panels while the lidar image shows several strong backscattering layers not prominent in the radar reflectivities. These layers also appear to largely attenuate the lidar returns so that in general no useful lidar signal is present below about 2.0 km.

The lower panels of Fig. (4) show the estimated lidar/radar effective particle size and the estimated water contents. The C-130 flights on this day show that layers of liquid water were often present over and around Chilbolton. However, little water was encountered during the coincident C-130 flight at 4.6 km. The inversion results shown here were conducted assuming that the strong backscattering layers below about 3.25 km (T=-4 Degrees Celsius) were comprised mainly of liquid water while elsewhere it was assumed that the clouds were ice. If an inversion is conducted assuming ice everywhere then the inferred particle sizes in these layers are still quite small (less than 2-4 microns). Since the far-end boundary values used in the inversions were set at the altitudes of these layers, assuming they are mainly ice instead of water alters the particle sizes and IWCs inferred for altitudes closer to the aircraft by 10–20%.

The separation in space and time as a function of latitude between the ARAT and the UKMO C-130 are shown in Fig. (5). It can be seen that within about 10km of Chilbolton the horizontal separation of the two aircraft was within 300 meters and the time difference within half a minute. Such separations are not ideal but given the large extent and high apparent stability of the large ice cloud sampled here together with the horizontal resolution of the aircraft measurements (about 500-600 meters for the C-130 measurements) they may be considered adequate for useful comparison in this case.

A comparison between various cloud properties inferred from the 2D probe measurements and the lidar/radar inversion results is shown in Fig. (6). The lidar/radar results shown are for an altitude of 4.55 km which was the maximum height at which reliable data was obtained. The C-130 flew at an altitude of around 4.6 Km which is just slightly higher than the maximum height of the lidar/radar data but is within one range bin (the resolution of the lidar data was 60 meters) of the top of the lidar/radar data. As before, results for the two different ways of interpreting the 2D probe data are presented except for the case of the inferred extinction. Since the optical extinction inferred from the 2D probes is just twice the cross-sectional area of the particles, the area binned 2D probe results for extinction are considered to be more accurate than those that may be inferred from the average dimension spectra. The lidar/radar IWC and R_{eff} estimates shown here were generated using the complex polycrystal model of

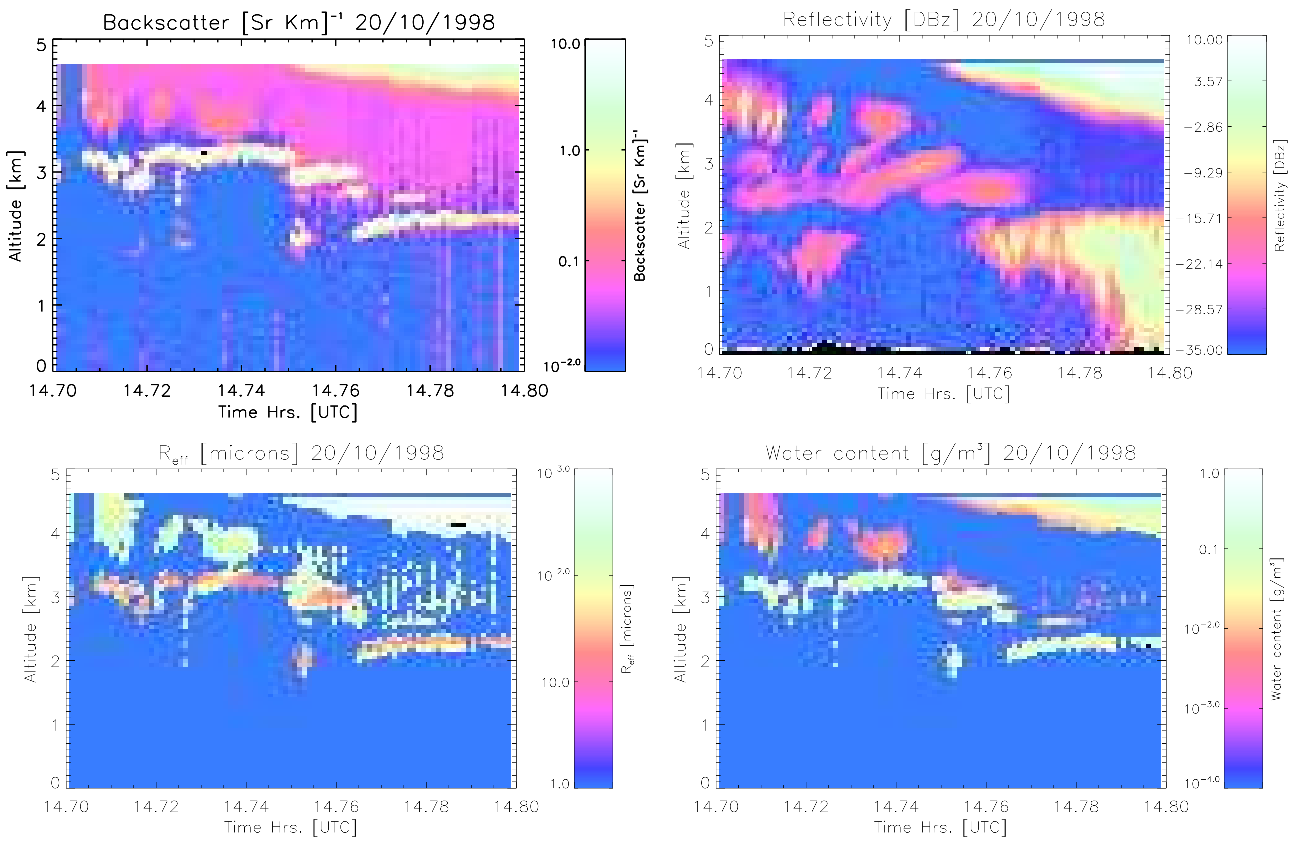

Figure 4: Observed radar reflectivity and lidar backscatter signal (top) together with the results of the lidar/radar inversion (bottom) for the ARAT flight path.

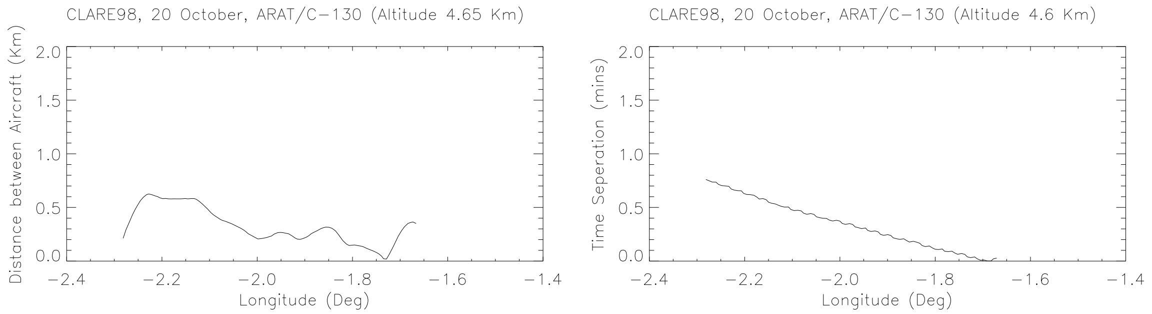

Figure 5: Separation in space and time between the ARAT and the UKMO C-130 as a function of latitude.

Mitchel et al. (1996). It should be noted that this model specifies a different mass-vs-area relationship than either of the two approaches used to interpret the 2D probe data.

The comparisons between the lidar/radar derived quantities and the 2D probe measurements are seen to be consistent within the uncertainty between the two methods for determining particle mass. In particular, the lidar/radar results for IWC appear to agree somewhat better for most of the flight path with the maximum dimension derived 2D probe estimates. The significance of this result is unclear at this point. A more rigorous comparison should be made which would incorporate the same mass-vs-area relationship in the lidar/radar retrievals as that used in the 2D probe estimates.

Conclusion

The agreement obtained between the remotely derived and in-situ derived cloud properties presented here is impressive, especially considering the diversity of the two approaches and the many possible sources of uncertainty inherent in both the lidar/radar retrieval process and the interpretation of the 2D probe images. It re-

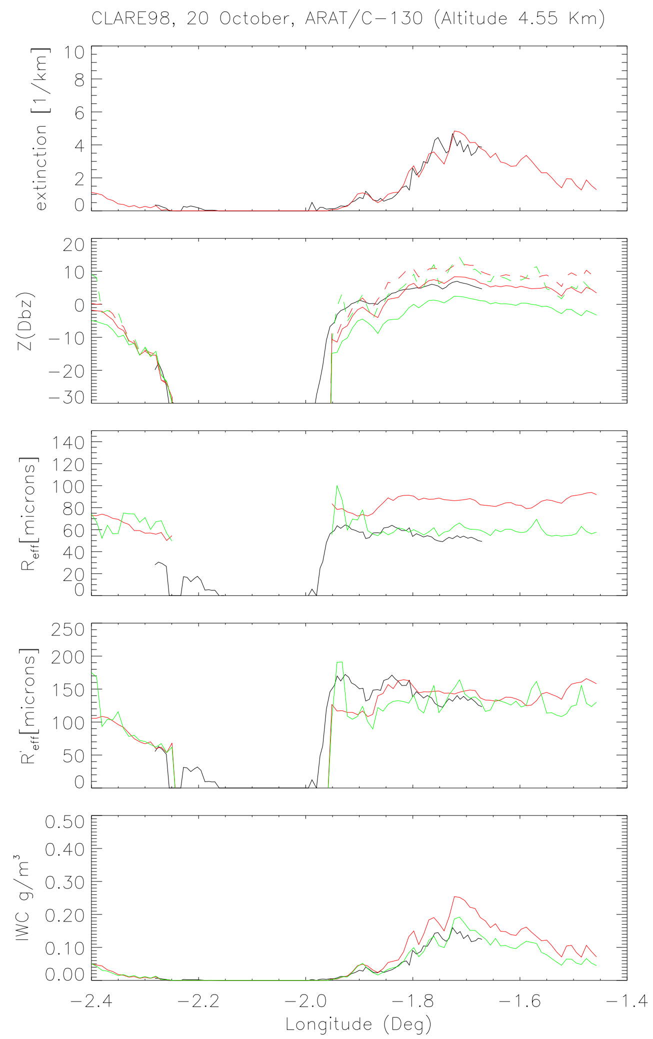

Figure 6: Comparison of lidar/radar results and 2D probe results for the ARAT/C-130 flight path. The black-solid lines show the respective results from the lidar/radar inversions at 4.55 km. The red lines show the respective results for the 2D probe data using the mass-vs-area relationship while the green lines show the respective results of the mass-vs-maximum average dimension relationship. In the panel showing the Z values, the dashed lines show the reflectivities calculated from the 2D probe data assuming Rayleigh scattering while the solid lines show the values calculated using Mie theory for spheres with the same cross-sectional area and mass as given by the 2D-probes.

mains to be seen whether such agreement is to be commonly expected or is limited to certain special circumstances.

Further work should be preformed to investigate the validity of the approximate treatment of non-spherical particle scattering implicitly used in the lidar/radar inversion process. As well, better characterization of the nature of proper mass-vs-area relationships for ice crystals would benefit both the interpretation of 2D probe data as well as aid in the accurate inversion of combined lidar and radar data.

References

Donovan, D.P., J. Goddard, H. Savageot and R.J. Hogan. Cloud effective radius and water contents inferred from combined lidar and radar observations during CLARE98, *this report*, (1999).

Donovan, D.P, and A.C.A.P. Van Lammeren, Combined lidar and radar cloud particle effective size retrievals made during CLARA, to appear in, *Phys. and Chem. of the Earth* (1999).

Eloranta, E.W., Practical model for the calculation of multiply scattered lidar returns, *Appl. Opts.*,**37**, 2464-2472 (1998).

Francis, P.N., A summary of the cloud microphysics data collected during CLARE'98 by the UKMO C-130 Aircraft, em this report (1999).

Goddard J.W.F., Performance of the Ground-based instruments at Chilbolton, *This Report*, (1999).

Guyot, A., J. Testud, O. Danne, M. Quante, and P. Francis, Calibration of the University of Wyoming 95 GHz airborne radar during CLARE'98, *This Report*, (1999a).

Guyot, A., J. Testud, J. Pelon, V. Trouillet, and P. Francis Synergy in ice clouds between airborne nadir pointing radar and lidar during CLARE'98 *This Report*, (1999b).

Mitchell, D.L., A. Macke, and Y. Liu, Modeling Cirrus Clouds. Part II: Treatment of Radiative Properties, *J. Atmos. Sci.*, **53**, 2967-2988 (1996).

Danne, O., and M. Quante, The GKSS 95 GHz cloud radar during CLARE 98: System performance and data products, *This Report*, (1999).